*Mineralogical Magazine* (2020), **84**, 153–158
doi:10.1180/mgm.2019.68

CAMBRIDGE UNIVERSITY PRESS

**Article**

# Majzlanite, $K_2Na(ZnNa)Ca(SO_4)_4$, a new anhydrous sulfate mineral with complex cation substitutions from Tolbachik volcano

Oleg I. Siidra[1,2*], Evgeny V. Nazarchuk[1], Anatoly N. Zaitsev[3] and Vladimir V. Shilovskikh[4]

[1]Department of Crystallography, St. Petersburg State University, University Embankment 7/9, 199034 St. Petersburg, Russia; [2]Kola Science Center, Russian Academy of Sciences, Apatity, Murmansk Region, 184200 Russia; [3]Department of Mineralogy, St. Petersburg State University, University Embankment 7/9, 199034 St. Petersburg, Russia; and [4]Geomodel Centre, St. Petersburg State University, University Embankment 7/9, 199034 St. Petersburg, Russia

**Abstract**

A new mineral majzlanite, ideally $K_2Na(ZnNa)Ca(SO_4)_4$, was found in high-temperature exhalative mineral assemblages in the Yadovitaya fumarole, Second scoria cone of the Great Tolbachik Fissure Eruption (1975–1976), Tolbachik volcano, Kamchatka Peninsula, Russia. Majzlanite is associated closely with langbeinite and K-bearing thénardite. Majzlanite is grey with a bluish tint, has a white streak and vitreous lustre. The mineral is soluble in warm water. Majzlanite is monoclinic, $C2/c$, $a = 16.007(2)$, $b = 9.5239(11)$, $c = 9.1182(10)$ Å, $\beta = 94.828(7)°$, $V = 1385.2(3)$ Å$^3$ and $Z = 16$. The eight strongest lines of the X-ray powder diffraction pattern are [*d*, Å (*I*, %)(*hkl*)]: 3.3721(40)($\bar{3}12$), 3.1473(56)($\bar{4}02$), 3.1062(65)($\bar{2}22$), 2.9495(50)($\bar{1}31$), 2.8736(100)($\bar{1}13$), 2.8350(70)(421), 2.8031(45)(511) and 2.6162(41)($\bar{5}12$). The following structural formula was obtained: $K_2Na(Zn_{0.88}Na_{0.60}Cu_{0.36}Mg_{0.16})(Ca_{0.76}Na_{0.24})(S_{0.98}Al_{0.015}Si_{0.005}O_4)_4$. The chemical composition determined by electron-microprobe analysis is (wt.%): $Na_2O$ 9.73, $K_2O$ 15.27, ZnO 11.20, CaO 7.03, CuO 4.26, MgO 1.07, $Al_2O_3$ 0.47, $SO_3$ 51.34, $SiO_2$ 0.12, total 100.49. The empirical formula calculated on the basis of 16 O apfu is $K_{1.99}Na_{1.93}Zn_{0.84}Ca_{0.77}Cu_{0.33}Mg_{0.16}(S_{3.94}Al_{0.06}Si_{0.01})O_{16}$ and the simplified formula is $K_2Na(Zn,Na,Cu,Mg)_{\Sigma2}(Ca,Na)(SO_4)_4$. No natural or synthetic compounds directly chemically and/or structurally related to majzlanite are known to date. The topology of the heteropolyhedral framework in majzlanite is complex. An interesting feature of the structure of majzlanite is an edge-sharing of $ZnO_6$ octahedra with $SO_4$ tetrahedra.

**Keywords:** majzlanite, new minerals, sulfates, framework structures, zinc, Tolbachik volcano

(Received 17 August 2019; accepted 17 October 2019; Accepted Manuscript published online: 22 October 2019; Associate Editor: Ian T. Graham)

## Introduction

Sulfate minerals with transition and/or alkali metals are represented typically by hydrated species (Hawthorne *et al.*, 2000). Anhydrous sulfate minerals with transition metal cations are mainly restricted to active fumaroles with strongly oxidising environments (Vergasova and Filatov, 2012; Balić-Žunić, *et al.*, 2016; Siidra *et al.*, 2017; Pekov *et al.*, 2018; Siidra *et al.*, 2019*a*). Our mineralogical investigations of the fumaroles of Tolbachik volcano over the last few years have revealed a number of new anhydrous sulfate mineral species: markhininite $TlBi(SO_4)_2$ (Siidra *et al.*, 2014); puninite $Na_2Cu_3O(SO_4)_3$ (Siidra *et al.*, 2017); hermannjahnite $CuZn(SO_4)_2$ (Siidra *et al.* 2018*b*); saranchinaite $NaCu(SO_4)_2$ (Siidra *et al.*, 2018*a*; Kovrugin *et al.*, 2019); belousovite $KZn(SO_4)Cl$ (Siidra *et al.*, 2018*c*); itelmenite $Na_2CuMg_2(SO_4)_4$ (Nazarchuk *et al.*, 2018); koryakite $NaKMg_2Al_2(SO_4)_6$ (Siidra *et al.*, 2019*b*) and glikinite $Zn_3O(SO_4)_2$ (Nazarchuk *et al.*, 2019).

Herein we report on the chemical composition, structure and properties of majzlanite (Cyrillic: майзланит), $K_2Na(ZnNa)Ca(SO_4)_4$. Majzlanite is named in honour of Prof Dr Juraj Majzlan (b. 1973). Juraj Majzlan works in the Institute of Geosciences, Friedrich-Schiller-University, Jena. In addition to other many achievements and contributions in the fields of mineralogy and crystallography, Juraj Majzlan has made significant contribution to the mineralogy of sulfates (see e.g. Majzlan *et al.*, 2017; Zittlau *et al.*, 2013; Grevel *et al.*, 2012).

Both the mineral and the mineral name were approved by the Commission on New Minerals, Nomenclature and Classification of the International Mineralogical Association (IMA2018-016, Siidra *et al.*, 2018*d*). Type material is deposited at the Mineralogical Museum, St. Petersburg State University, St. Petersburg, Russia (catalogue no. 1/19690).

## Occurrence and association

Majzlanite occurs as a product of fumarolic activity. It was found in June 2016, in the Yadovitaya fumarole, Second scoria cone, Northern Breakthrough (North Breach), Great Fissure eruption, Tolbachik volcano, Kamchatka, Russia. The Second Scoria Cone is located ~18 km SSW of the active shield volcano Ploskiy Tolbachik (Fedotov and Markhinin, 1983). Majzlanite is associated closely with langbeinite (Fig. 1), thénardite (Fig. 2) and euchlorine. The temperature of gases at the sampling location was ~300°C. All the samples recovered were packed immediately and isolated to avoid any contact with the external atmosphere.

*Author for correspondence: Oleg I. Siidra, Email: o.siidra@spbu.ru
**Cite this article:** Siidra O.I., Nazarchuk E.V., Zaitsev A.N. and Shilovskikh V.V. (2020) Majzlanite, $K_2Na(ZnNa)Ca(SO_4)_4$, a new anhydrous sulfate mineral with complex cation substitutions from Tolbachik volcano. *Mineralogical Magazine* **84**, 153–158. https://doi.org/10.1180/mgm.2019.68

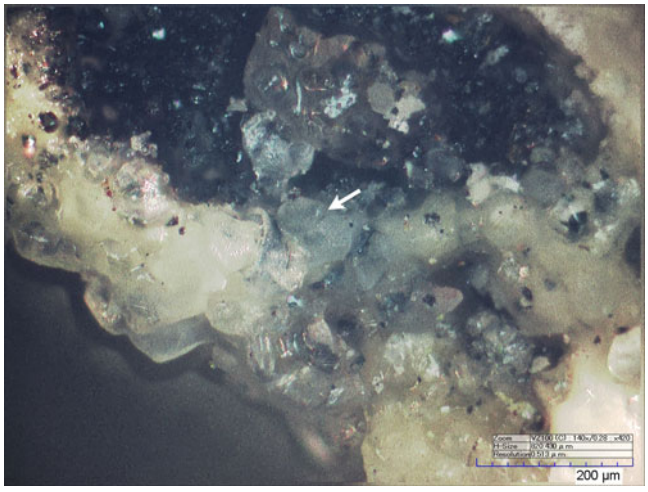


**Fig. 1.** Bluish-white transparent crystals of majzlanite (marked by a white arrow) in association with langbeinite in the voids of basaltic scoria.

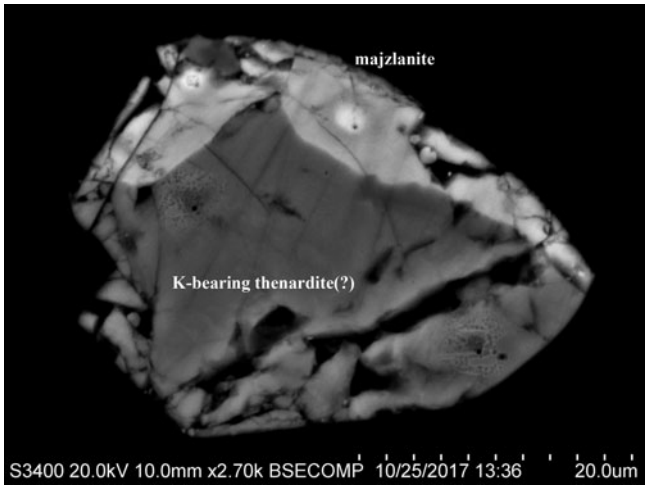


**Fig. 2.** Back-scattered electron image. Majzlanite rim (light grey) on K-bearing thénardite(?) (dark grey). White areas within majzlanite and spotted areas within K-bearing thénardite (?) are surface damage by an electron beam.

**Table 1.** Analytical data (wt.%) for majzlanite.

| Constituent | Mean | Range | S.D. | Probe standard |
|---|---|---|---|---|
| $Na_2O$ | 9.73 | 9.10–10.50 | 0.58 | NaCl |
| $K_2O$ | 15.27 | 14.70–15.52 | 0.34 | KCl |
| ZnO | 11.20 | 10.73–11.88 | 0.42 | Zn |
| CaO | 7.03 | 6.49–7.43 | 0.40 | $Ca(SO_4)$ |
| CuO | 4.26 | 3.92–4.78 | 0.38 | Cu |
| MgO | 1.07 | 0.99–1.18 | 0.07 | MgO |
| $Al_2O_3$* | 0.47 | 0.43–0.49 | 0.03 | $Al_2O_3$ |
| $SO_3$ | 51.34 | 50.39–52.07 | 0.64 | $Ca(SO_4)$ |
| $SiO_2$ | 0.12 | 0.03–0.15 | 0.05 | $SiO_2$ |
| Total | 100.49 | | | |

*Mean of three analyses.
S.D. – standard deviation

## Physical properties

Majzlanite occurs in the voids of volcanic scoria (Fig. 1) associated closely with langbeinite as irregular grains up to 50 µm × 50 µm × 80 µm. Majzlanite is grey with a bluish tint (Fig. 1), has a white streak and vitreous lustre. The mineral is brittle with uneven fracture. Cleavage or parting was not observed. Hardness corresponds to 2–3 on the Mohs' scale. The density could not be measured due to the lack of suitable sample, but was calculated as 2.961 g $cm^{-3}$ using structural data and the empirical formula. No fluorescence was detected.

Optical properties could not be measured because of thin intergrowths of majzlanite with K-bearing thénardite(?) (Fig. 2). Majzlanite is soluble in warm $H_2O$.

**Table 2.** Powder X-ray diffraction data (*d* in Å) for majzlanite.

| $I_{calc}$ | $I_{meas}$ | $d_{calc}$ | $d_{meas}$ | *hkl* | $I_{calc}$ | $I_{meas}$ | $d_{calc}$ | $d_{meas}$ | *hkl* |
|---|---|---|---|---|---|---|---|---|---|
| 48 | 14 | 4.7620 | 4.7181 | 020 | **45** | **41** | **2.6160** | **2.6162** | **$\bar{5}12$** |
| 5 | 1 | 4.6424 | 4.6487 | 310 | 3 | 2 | 2.4638 | 2.4569 | 422 |
| 15 | 2 | 4.5429 | 4.5449 | 002 | 1 | 2 | 2.4300 | 2.4334 | 512 |
| 1 | 2 | 4.2629 | 4.2383 | $\bar{3}11$ | 1 | 1 | 2.3212 | 2.3166 | 620 |
| 21 | 18 | 4.0460 | 4.0461 | $\bar{1}12$ | 1 | 4 | 2.2715 | 2.2784 | 004 |
| 10 | 31 | 4.0162 | 4.0224 | 311 | 2 | 1 | 2.2347 | 2.2286 | $\bar{2}04$ |
| 1 | 5 | 3.9004 | 3.9416 | 112 | 1 | 2 | 2.2134 | 2.2199 | $\bar{1}14$ |
| 35 | 7 | 3.6697 | 3.6541 | 221 | 5 | 1 | 2.1890 | 2.1949 | $\bar{1}33$ |
| **41** | **40** | **3.3732** | **3.3721** | **$\bar{3}12$** | 16 | 4 | 2.1546 | 2.1533 | 531 |
| 38 | 4 | 3.2870 | 3.2953 | 022 | 2 | 3 | 2.1089 | 2.1118 | 042 |
| 41 | 30 | 3.1338 | 3.1331 | 312 | 1 | 1 | 2.0596 | 2.0560 | 513 |
| **40** | **56** | **3.1303** | **3.1473** | **$\bar{4}02$** | 41 | 32 | 2.0230 | 2.0227 | $\bar{2}24$ |
| **79** | **65** | **3.1064** | **3.1062** | **$\bar{2}22$** | 1 | 6 | 2.0194 | 2.0213 | 242 |
| 43 | 3 | 3.0249 | 3.0073 | 510 | 1 | 1 | 1.9763 | 1.9756 | 441 |
| **98** | **50** | **2.9604** | **2.9495** | **$\bar{1}31$** | 6 | 1 | 1.9502 | 1.9384 | 224 |
| **100** | **100** | **2.8808** | **2.8736** | **$\bar{1}13$** | 1 | 1 | 1.8902 | 1.8915 | $\bar{5}14$ |
| **90** | **70** | **2.8427** | **2.8350** | **421** | 1 | 1 | 1.8626 | 1.8639 | $\bar{7}13$ |
| **59** | **45** | **2.8038** | **2.8031** | **511** | 15 | 8 | 1.8348 | 1.8329 | 442 |
| 27 | 15 | 2.7257 | 2.7150 | 330 | 1 | 1 | 1.8035 | 1.8008 | $\bar{6}04$ |
| 9 | 33 | 2.6423 | 2.6483 | $\bar{3}31$ | | | | | |

## Chemical composition

One grain, 21 µm × 13 µm in size (Fig. 2) with majzlanite as a rim on K-bearing thénardite(?), was analysed by energy-dispersive spectrometry using a Hitachi S-3400N scanning electron microscope equipped with an Oxford Instruments X-Max 20 Energy Dispersive Spectrometer. The electron-beam accelerating voltage was 20 kV and the current 1.8 nA. A defocused beam (up to 4 µm spot size) was used and the X-ray acquisition time was 30 s. The mineral is unstable under the electron beam and back-scattered electron images show strong damage of the mineral surface (Fig. 2). Analytical data are given in Table 1.

The empirical formula calculated on the basis of 16 O atoms per formula unit is $K_{1.99}Na_{1.93}Zn_{0.84}Ca_{0.77}Cu_{0.33}Mg_{0.16}(S_{3.94}Al_{0.06}Si_{0.01})O_{16}$ and the simplified formula is $K_2Na(Zn,Na,Cu,Mg)_{\Sigma 2}(Ca,Na)(SO_4)_4$.

The ideal formula, taking into account structural data and charge balance is $K_2Na(ZnNa)Ca(SO_4)_4$, which requires $K_2O$ 15.34, $Na_2O$ 10.10, ZnO 13.26, CaO 9.13, $SO_3$ 52.17, total 100.00 wt.%.

## X-ray crystallography

### *Experiment*

Powder X-ray studies were done using a Rigaku R-Axis Rapid II diffractometer with a cylindrical image-plate detector, with Co*K*α radiation. For the powder-diffraction study, a Gandolfi-like motion on the φ and ω axes was used to randomise the sample and observed *d* values and intensities were derived by *osc2xrd* software (Britvin *et al.*, 2017). The powder data are presented in Table 2. Unit-cell parameters refined from the powder data are:

https://doi.org/10.1180/mgm.2019.68 Published online by Cambridge University Press

$a = 15.9775(9)$ Å, $b = 9.5196(5)$, $c = 9.1216(4)$ Å, $\beta = 94.921(4)°$ and $V = 1382.29(8)$ Å$^3$.

A transparent prismatic crystal fragment of majzlanite was mounted on a thin glass fibre for X-ray diffraction analysis using a Bruker APEX II DUO X-ray diffractometer with a micro-focus X-ray tube operated with Mo*K*α radiation at 50 kV and 40 mA. The data were integrated and corrected for absorption using a multi-scan type model implemented in the Bruker programs *APEX* and *SADABS* (Bruker-AXS, 2014). More than a hemisphere of X-ray diffraction data was collected. The structure was solved by direct methods and was refined using *SHELXL* software (Sheldrick, 2015). All of the atoms were refined anisotropically. Details of data collection and structure refinement are provided in Table 3. Bond-valence sums, fractional coordinates and atom-displacement parameters are provided in Table 4 and selected interatomic distances in Table 5. All bond-valence parameters were taken from Brese and O'Keeffe (1991). Taking into account multiple cation substitutions, the bond-valence sums are in good agreement with the expected oxidation states. The crystallographic information files have been deposited with the Principal Editor of *Mineralogical Magazine* and are available as Supplementary material (see below).

**Table 3.** Crystallographic data and refinement parameters for majzlanite.

| | |
|---|---|
| **Crystal data** | |
| Ideal formula | $K_2Na(ZnNa)Ca(SO_4)_4$ |
| Crystal dimensions (mm) | 0.07 × 0.07 × 0.09 |
| Crystal system, space group | monoclinic, *C*2/*c* |
| Temperature (K) | 296 |
| *a*, *b*, *c* (Å) | 16.007(2), 9.5239(11), 9.1182(10) |
| β (°) | 94.828(7) |
| *V* (Å$^3$) | 1385.2(3) |
| *Z* | 16 |
| $D_{calc}$ (g/cm$^3$) | 2.973 |
| μ (mm$^{-1}$) | 3.823 |
| **Data collection** | |
| Instrument | Bruker Apex 2 Duo |
| Radiation type, wavelength (Å) | Mo*K*α, 0.71073 |
| θ range (°) | 2.491–23.924 |
| No. of measured, independent and observed [$\|Fo\| \geq 4s_F$] reflections | 8261, 1081, 855 |
| $R_{int}$ | 0.063 |
| Indices range of *h*, *k*, *l* | $-18 \leq h \leq 18$, $-10 \leq k \leq 10$, $-10 \leq l \leq 10$ |
| **Refinement** | |
| $R_1$, $wR_2$ | 0.030, 0.052 |
| $R_1$ all, $wR_2$ all | 0.047, 0.058 |
| GoF | 1.050 |
| Weighting coefficients *a*, *b* | 0.015200, 4.777200 |
| Data/restraints/parameters | 855/0/123 |
| $\Delta\rho_{max}$, $\Delta\rho_{min}$ ($e^-$ Å$^{-3}$) | +0.374, −0.438 |

## Crystal structure

### *Cation coordination*

The crystal structure of majzlanite contains one symmetrically independent K site, one Zn, one Na, one Ca and two S cation sites. The K site is coordinated by 11 O atoms, forming the irregular polyhedron shown in Fig. 3. The Na forms $NaO_6$ octahedra. During the process of crystal structure refinement, it was found that K and Na sites are occupied exclusively by $K^+$ and $Na^+$ cations, respectively (Table 4).

The Zn site has a distorted octahedral environment and mixed occupancy by $Zn^{2+}$, $Na^+$, $Cu^{2+}$ and $Mg^{2+}$ (Table 4). As the X-ray scattering power of Na and Mg atoms is indistinguishable, Na and Mg were regarded as one group with one scattering factor. Na and Mg atoms were summed to form Na* in the atom fraction. For the same reason, $Zn^{2+}$ and $Cu^{2+}$ were assumed to constitute Zn*. Replacement of $Zn^{2+}$ by $Na^+$ is unusual. Previously the similar substitution was found in synthetic alluaudite-related material, $Na(Na_{0.6}Zn_{0.4})Zn_2(H_{0.6}AsO_4)(AsO_3OH)_2$ (Đorđević *et al.*, 2015) and in paseroite (Mills *et al.*, 2012).

The Ca site coordination environments can be described as a strongly distorted $CaO_6$ octahedron. Refinement of the occupancy of the Ca site reveals the presence of minor $Na^+$ (Table 4).

Two S sites with the site-scattering values are compatible with occupancy by $S^{6+}$ and tetrahedrally coordinated by O anions. $SO_4$ groups exhibit the usual tetrahedral distances and angles. The <S–O> distances demonstrate similar values of ~1.46 Å and ~1.47 Å, which are in a good agreement with the <S–O> distance of 1.473 Å reported for sulfate minerals by Hawthorne *et al.* (2000). The minor amount of $Al^{3+}$ and $Si^{4+}$ detected by microprobe in tetrahedral S sites plays an important role as a charge compensating agent. The content of $Al^{3+}$ and $Si^{4+}$ was fixed in agreement with the microprobe data reported above.

The following structural formula was obtained: $K(Zn_{0.44}Na_{0.30}Cu_{0.18}Mg_{0.08})(Na_{0.5})(Ca_{0.38}Na_{0.12})(S_{0.98}Al_{0.015}Si_{0.005}O_4)_2$ which is in excellent agreement with that obtained by microprobe analysis.

**Table 4.** Bond-valence sums, coordinates, anisotropic and isotropic displacement parameters (Å$^2$) of atoms in majzlanite.

| Atom | Site | B.V.S. | *x* | *y* | *z* | $U_{eq}$ | $U^{11}$ | $U^{22}$ | $U^{33}$ | $U^{23}$ | $U^{13}$ | $U^{12}$ |
|---|---|---|---|---|---|---|---|---|---|---|---|---|
| K | 8*f* | 1.12 | 0.38480(7) | 0.94023(10) | 0.17873(10) | 0.0298(3) | 0.0356(7) | 0.0248(6) | 0.0287(6) | 0.0008(4) | 0.0003(5) | 0.0008(5) |
| Zn* | 8*f* | 1.66 | 0.13799(4) | 0.80138(7) | 0.17300(7) | 0.0204(3) | 0.0163(5) | 0.0262(5) | 0.0185(4) | 0.0002(3) | 0.0006(3) | 0.0018(3) |
| Na | 4*c* | 1.05 | ¼ | ¾ | ½ | 0.0271(6) | 0.0281(16) | 0.0294(14) | 0.0231(12) | 0.0003(11) | −0.0021(11) | −0.0019(12) |
| Ca** | 4*e* | 2.00 | 0 | 0.93271(15) | −¼ | 0.0359(7) | 0.0265(11) | 0.0175(10) | 0.0660(12) | 0 | 0.0173(8) | 0 |
| S1*** | 8*f* | 6.22 | 0.20869(7) | 0.09183(11) | 0.35118(11) | 0.0220(3) | 0.0188(7) | 0.0231(6) | 0.0244(6) | 0.0031(5) | 0.0040(5) | 0.0003(5) |
| S2*** | 8*f* | 6.14 | −0.02782(8) | 0.74073(12) | 0.04369(11) | 0.0244(3) | 0.0251(8) | 0.0335(7) | 0.0144(5) | −0.0003(5) | 0.0015(5) | −0.0016(6) |
| O1 | 8*f* | 2.12 | 0.2466(2) | 0.6917(3) | 0.2380(3) | 0.0394(9) | 0.038(2) | 0.054(2) | 0.0277(16) | −0.0137(17) | 0.0075(15) | 0.0178(18) |
| O2 | 8*f* | 2.12 | −0.1086(2) | 0.7243(3) | 0.1087(3) | 0.0316(8) | 0.022(2) | 0.040(2) | 0.0329(17) | 0.0072(15) | 0.0002(15) | −0.0061(16) |
| O3 | 8*f* | 1.99 | 0.2674(2) | 0.9997(3) | 0.4326(3) | 0.0402(9) | 0.034(2) | 0.037(2) | 0.047(2) | 0.0074(17) | −0.0090(17) | 0.0104(17) |
| O4 | 8*f* | 2.04 | 0.1600(2) | 0.1741(3) | 0.4485(4) | 0.0474(10) | 0.050(3) | 0.042(2) | 0.056(2) | 0.0081(18) | 0.0320(19) | 0.0126(19) |
| O5 | 8*f* | 1.96 | 0.0312(2) | 0.6300(4) | 0.0929(3) | 0.0453(10) | 0.049(3) | 0.058(2) | 0.0288(17) | 0.0109(17) | 0.0038(16) | 0.026(2) |
| O6 | 8*f* | 2.11 | 0.1502(2) | 0.0117(3) | 0.2510(4) | 0.0479(10) | 0.040(2) | 0.045(2) | 0.054(2) | 0.0053(19) | −0.0187(18) | −0.0081(18) |
| O7 | 8*f* | 2.22 | −0.0415(2) | 0.7396(4) | −0.1160(3) | 0.0462(11) | 0.063(3) | 0.062(2) | 0.0125(16) | 0.0026(16) | −0.0049(16) | 0.011(2) |
| O8 | 8*f* | 2.12 | 0.0106(2) | 0.8750(4) | 0.0932(4) | 0.0522(11) | 0.053(3) | 0.046(2) | 0.062(2) | −0.025(2) | 0.034(2) | −0.029(2) |

*$Zn_{0.621(4)}Na_{0.379(4)}$ where Zn = $Zn_{0.44}$ + $Cu_{0.18}$ and Na = $Mg_{0.08}$ + $Na_{0.30}$; **$Ca_{0.758(11)}Na_{0.242(11)}$;*** $S_{0.98}Al_{0.015}Si_{0.005}$. Bond-valence sums (BVS) for mixed sites were calculated using parameters for Zn–O and Ca–O bonds from Brese and O'Keeffe (1991).

https://doi.org/10.1180/mgm.2019.68 Published online by Cambridge University Press

**Table 5.** Selected interatomic distances (Å) in majzlanite.

| | | | |
|---|---|---|---|
| K–O7 | 2.730(3) | Zn–O1 | 2.072(3) |
| K–O2 | 2.784(3) | Zn–O4 | 2.119(3) |
| K–O4 | 2.853(3) | Zn–O6 | 2.129(3) |
| K–O3 | 2.862(3) | Zn–O2 | 2.209(3) |
| K–O5 | 2.989(3) | Zn–O8 | 2.220(4) |
| K–O5 | 2.992(3) | Zn–O5 | 2.431(4) |
| K–O5 | 3.111(4) | | |
| K–O7 | 3.130(4) | S1–O3 | 1.444(3) |
| K–O3 | 3.154(4) | S1–O4 | 1.458(3) |
| K–O1 | 3.314(4) | S1–O6 | 1.466(3) |
| K–O1 | 3.318(4) | S1–O1 | 1.475(3) |
| | | <S1–O> | 1.460 |
| Na–O2 | 2.406(3) ×2 | | |
| Na–O1 | 2.449(3) ×2 | S2–O7 | 1.454(3) |
| Na–O3 | 2.478(3) ×2 | S2–O5 | 1.461(3) |
| | | S2–O8 | 1.473(3) |
| Ca–O7 | 2.336(4) ×2 | S2–O2 | 1.475(3) |
| Ca–O8 | 2.339(3) ×2 | <S2–O> | 1.470 |
| Ca–O6 | 2.461(4) ×2 | | |

### *Structure description*

The topology of framework in majzlanite is complicated. $NaO_6$ and $CaO_6$ octahedra are connected to sulfate tetrahedra via common corners (Fig. 3). $ZnO_6$ octahedra link to $SO_4$ tetrahedra via both common corners and edges. Due to this fact, Zn–O5 and Zn–O8 bonds are elongated (Table 5) in the $ZnO_6$ octahedron. The Zn–S2 distance in majzlanite is 2.8704(4) Å. Edge-sharing between sulfate tetrahedra and transition-metal octahedra is exceptionally rare. It has never been observed in zinc sulfates. The short Cu–S distance of 2.593 Å between $CuO_6$ octahedron shared via common edges with $SO_4$ group is observed in chlorothionite $K_2CuCl_2(SO_4)$ (Giacovazzo *et al.*, 1976). However, edge-sharing is common for $NaO_6$ octahedra and $SO_4$ tetrahedra (e.g. thénardite, $Na_2SO_4$: Hawthorne and Ferguson, 1975; tamarugite, $NaAl(H_2O)_6(SO_4)_2$: Mereiter, 2013). The Na–S distance is 2.965 Å in tamarugite and 3.112 Å in thénardite.

The $CaO_6$ octahedron shares two O6–O8 edges with two $ZnO_6$ octahedra, forming trimers (Fig. 4*a*). These trimers link to each other via corner- and edge-sharing with sulfate tetrahedra, forming complex rod-like one-dimensional units elongated along the *c* axis (Fig. 4*b*). Additionally, the rods are decorated by $NaO_6$ octahedra, which in turn share common edges with $ZnO_6$ octahedra (Figs 4*d*,*e*). Cavities in the framework are occupied by $K^+$ (Fig. 4*f*).

## Final remarks

The framework in majzlanite is unique among minerals and synthetic phases. Anhydrous sulfate compounds containing Zn, Na, K and Ca are unknown. Moreover, anhydrous Zn sulfates are

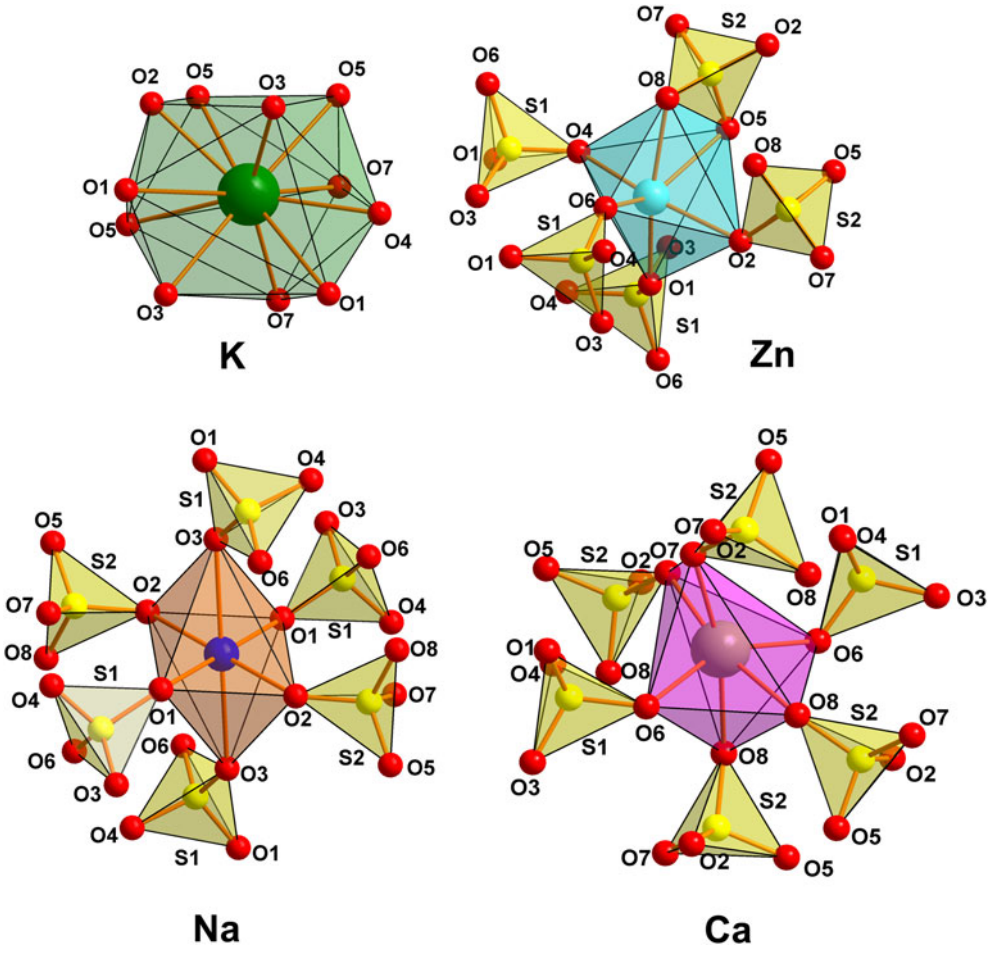


**Fig. 3.** Coordination environments of atoms in majzlanite.

https://doi.org/10.1180/mgm.2019.68 Published online by Cambridge University Press

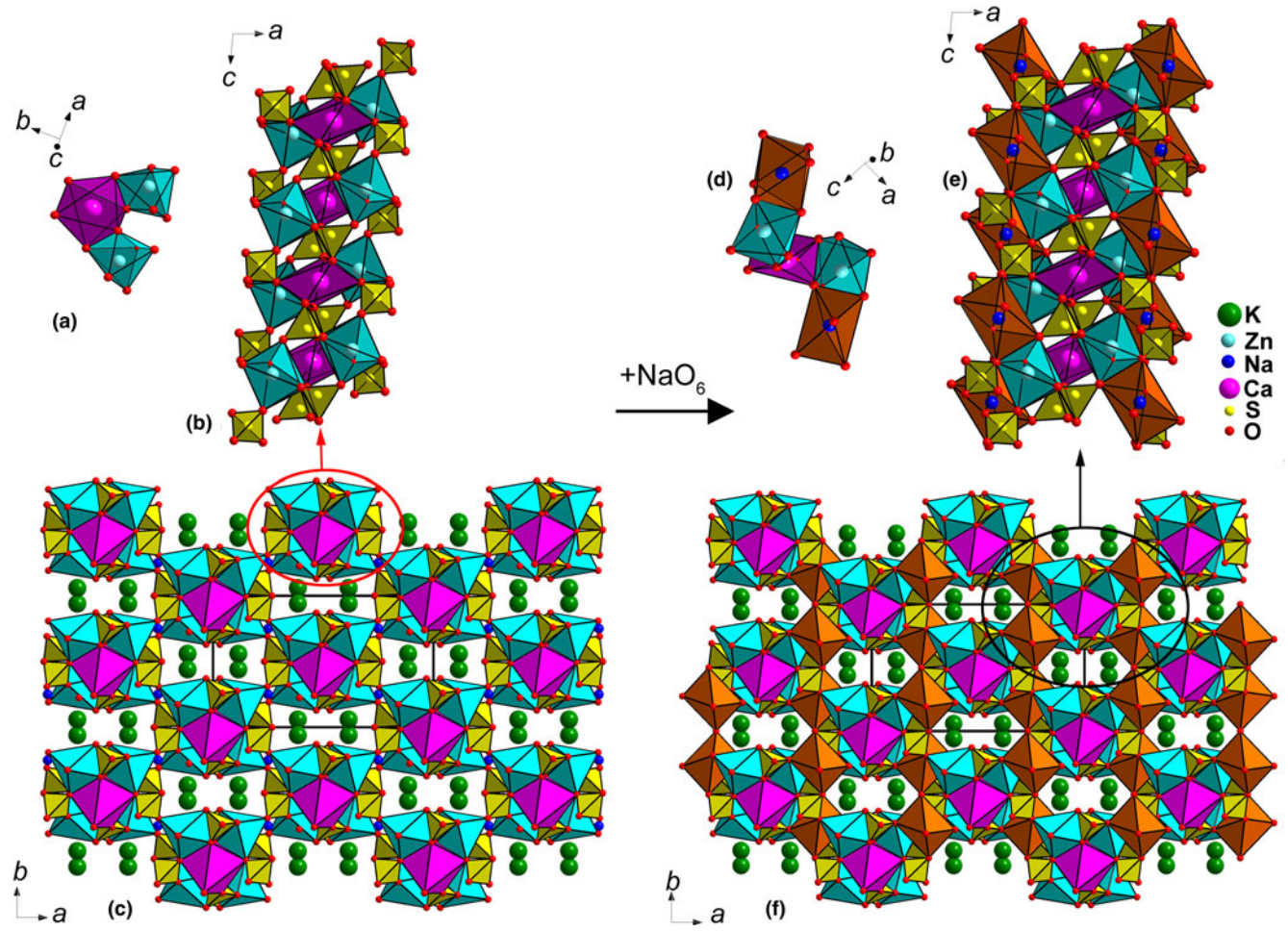


**Fig. 4.** (*a*) Trimeric units forming (*b*) rod like arrangements with (*c*) $SO_4$ tetrahedra in the structure of majzlanite. $CaO_6$ = pink; $ZnO_6$ = sky blue; and $SO_4$ = yellow. Channels are filled by K (green balls) and Na (blue balls) cations. (*d*, *e*, *f*) $NaO_6$ polyhedra (orange) are added. See the text for details.

exceptionally rare. Only three anhydrous Zn sulfates are known to date: hermannjahnite $CuZn(SO_4)_2$ (Siidra *et al.*, 2018*b*), glikinite $Zn_3O(SO_4)_2$ (Nazarchuk *et al.*, 2019) and belousovite $KZn(SO_4)Cl$ (Siidra *et al.*, 2018*c*). Majzlanite is distantly chemically related to itelmenite $Na_2CuMg_2(SO_4)_4$ (Nazarchuk *et al.*, 2018). The occurrence of zinkosite $ZnSO_4$ is doubtful to date (Wildner and Giester, 1988). However, given the widespread occurrence of chalcocyanite $CuSO_4$ in exhalative mineral assemblages (Siidra *et al.*, 2018*b*), zinkosite could also be found in Tolbachik fumaroles as a reliable mineral species. Queitite $Pb_4Zn_2(SO_4)(Si_2O_7)(SiO_4)$ (Hess and Keller, 1980) also contains sulfate anions, however the crystal structure is based on zinc-silicate layers with lead sulfate in the interlayer. Properties of queitite, such as poor solubility, are controlled mostly by silicate anions strongly bonded to $Zn^{2+}$ cations and $SO_4$ groups bonded with $Pb^{2+}$. A typical characteristic of all high-temperature fumarolic zinc sulfates listed above is their high solubility.

Multiple cation substitutions were also reported recently in the fumarolic sulfate philoxenite $(K,Na,Pb)_4(Na,Ca)_2(Mg,Cu)_3(Fe^{3+}_{0.5}Al_{0.5})(SO_4)_8$ (Pekov *et al.*, 2016). The structural architecture of philoxenite is completely different from majzlanite.

**Supplementary material.** To view supplementary material for this article, please visit https://doi.org/10.1180/mgm.2019.68

**Acknowledgements.** We are grateful to two anonymous reviewers and Peter Leverett for valuable comments. This work was financially supported by the Russian Science Foundation, grant no. 16-17-10085. Technical support by the SPbSU X-ray Diffraction and Geomodel Resource Centres is gratefully acknowledged.

## References

Balić-Žunić T., Garavelli A., Jakobsson S.P., Jonasson K., Katerinopoulos A., Kyriakopoulos K., Acquafredda P. (2016) Fumarolic minerals: An overview of active European volcanoes. Pp. 267–322 in: *Updates in Volcanology - From Volcano Modelling to Volcano Geology*. IntechOpen, London.

Brese N.E. and O'Keeffe M. (1991) Bond-valence parameters for solids. *Acta Crystallographica*, **B47**, 192–197.

Britvin S.N., Dolivo-Dobrovolsky D.V. and Krzhizhanovskaya M.G. (2017) Software for processing the X-ray powder diffraction data obtained from the curved image plate detector of Rigaku RAXIS Rapid II diffractometer. *Proceedings of the Russian Mineralogical Society*, **146**, 104–107.

Bruker-AXS (2014) *APEX2*. Version 2014.11-0. Madison, Wisconsin, USA.

Đorđević T., Wittwer A. and Krivovichev S.V. (2015) Three new alluaudite-like protonated arsenates: $NaMg_3(AsO_4)(AsO_3OH)_2$, $NaZn_3(AsO_4)(AsO_3OH)_2$ and $Na(Na_{0.6}Zn_{0.4})Zn_2(H_{0.6}AsO_4)(AsO_3OH)_2$. *European Journal of Mineralogy*, **27**, 559–573.

Fedotov S.A. and Markhinin Y.K. (editors) (1983) *The Great Tolbachik Fissure Eruption*. Cambridge Univ. Press, New York.

Giacovazzo C., Scandale E. and Scordari F. (1976) The crystal structure of chlorothionite $CuK_2Cl_2SO_4$. *Zeitschrift für Kristallographie – Crystalline Materials*, **144**, 226–237.

Grevel K.D., Majzlan J., Benisek A., Dachs E., Steiger M., Fortes A.D. and Marler, B. (2012) Experimentally determined standard thermodynamic properties of synthetic $MgSO_4{\cdot}4H_2O$ (Starkeyite) and $MgSO_4{\cdot}3H_2O$: a revised internally consistent thermodynamic data set for magnesium sulfate hydrates. *Astrobiology*, **12**, 1042–1054.

Hawthorne F.C. and Ferguson R.B. (1975) Anhydrous sulphates. I. Refinement of the crystal structure of celestite with an appendix on the structure of thenardite. *The Canadian Mineralogist*, **13**, 181–187.

Hawthorne F.C., Krivovichev S.V. and Burns P.C. (2000) The crystal chemistry of sulfate minerals. Pp. 1–112 in: *Sulfate Minerals: Crystallography, Geochemistry, and Environmental Significance* (C.N. Alpers, J.L. Jambor and D.K. Nordstrom, editors). Reviews in Mineralogy and Geochemistry, 40. The Mineralogical Society of America and the Geochemical Society, Washington DC.

Hess H. and Keller P. (1980) Die kristallstruktur von queitit, $Pb_4Zn_2(SO_4)(SiO_4)(Si_2O_7)$. *Zeitschrift für Kristallographie*, **151**, 287–299.

Kovrugin V.M., Nekrasova D.O., Siidra O.I., Mentré O., Masquelier C., Stefanovich S.Yu. and Colmont M. (2019) Mineral-inspired crystal growth and physical properties of $Na_2Cu(SO_4)_2$, and review of $Na_2M(SO_4)_2(H_2O)_x$ ($x = 0$–6) compounds. *Crystal Growth and Design*, **19**, 1233–1244.

Majzlan J., Grevel K.-D., Kiefer B. and Johnson M.B. (2017) Thermodynamics and crystal chemistry of rhomboclase, $(H_5O_2)Fe(SO_4)_2{\cdot}2H_2O$, and the phase $(H_3O)Fe(SO_4)_2$ and implications for acid mine drainage. *American Mineralogist*, **102**, 643–654.

Mereiter K. (2013) Redetermination of tamarugite, $NaAl(SO_4)_2{\cdot}6(H_2O)$. *Acta Crystallographica*, **E69**, i63–i64.

Mills S.J., Bindi L., Cadoni M., Kampf A.R., Ciriotti M.E., Ferraris G. (2012) Paseroite, $PbMn^{2+}(Mn^{2+},Fe^{2+})_2(V^{5+},Ti,Fe^{3+},\square)_{18}O_{38}$, a new member of the crichtonite group. *European Journal of Mineralogy*, **24**, 1061–1067.

Nazarchuk E.V., Siidra O.I., Agakhanov A.A., Lukina E.A., Avdontseva E.Y., Karpov G.A. (2018) Itelmenite, $Na_2CuMg_2(SO_4)_4$, a new anhydrous sulphate mineral from the Tolbachik volcano. *Mineralogical Magazine*, **82**, 1233–1241.

Nazarchuk E.V., Siidra O.I., Nekrasova D.O., Borisov A.S. and Shilovskikh V.V. (2019) Glikinite, IMA 2018-119. CNMNC Newsletter No. 47, February 2019, page 202; *European Journal of Mineralogy*, **31**, 199–204.

Pekov I.V., Zubkova N.V., Agakhanov A.A., Belakovskiy D.I., Vigasina M.F., Britvin S.N., Turchkova A.G., Sidorov E.G. and Pushcharovsky D.Y. (2016) Philoxenite, IMA 2015-108. CNMNC Newsletter No. 30, April 2016, page 410; *Mineralogical Magazine*, **80**, 407–413.

Pekov I.V., Zubkova N.V., Agakhanov A.A., Pushcharovsky D.Y., Yapaskurt V.O., Belakovskiy D.I., Vigasina M.F., Sidorov E.G. and Britvin S.N. (2018) Cryptochalcite, $K_2Cu_5O(SO_4)_5$, and cesiodymite, $CsKCu_5O(SO_4)_5$, two newisotypic minerals and the K–Cs isomorphism in this solid-solution series. *European Journal of Mineralogy*, **30**, 593–607.

Sheldrick G.M. (2015) Crystal structure refinement with SHELXL. *Acta Crystalographica*, **71**, 3–8.

Siidra O.I., Vergasova L.P., Krivovichev S.V., Kretser Y.L., Zaitsev A.N. and Filatov S.K. (2014) Unique thallium mineralization in the fumaroles of Tolbachik volcano, Kamchatka peninsula, Russia. I. Markhininite, $TlBi(SO_4)_2$. *Mineralogical Magazine*, **78**, 1687–1698.

Siidra O.I., Nazarchuk E.V., Zaitsev A.N., Lukina E.A., Avdontseva E.Y., Vergasova L.P., Vlasenko N.S., Filatov S.K., Turner R., Karpov G.A. (2017) Copper oxosulphates from fumaroles of Tolbachik Vulcano: puninite, $Na_2Cu_3O(SO_4)_3$ – a new mineral species and structure refinements of kamchatkite and alumoklyuchevskite. *European Journal of Mineralogy*, **29**, 499–510.

Siidra O.I., Lukina E.A., Nazarchuk E.V., Depmeier W., Bubnova R.S., Agakhanov A.A., Avdontseva E.Yu., Filatov S.K. and Kovrugin V.M. (2018a) Saranchinaite, $Na_2Cu(SO_4)_2$, a new exhalative mineral from Tolbachik Volcano, Kamchatka, Russia, and a product of the reversible dehydration of kröhnkite, $Na_2Cu(SO_4)_2(H_2O)_2$. *Mineralogical Magazine*, **82**, 257–274.

Siidra O.I., Nazarchuk E.V., Agakhanov A.A., Lukina E.A., Zaitsev A.N., Turner R., Filatov S.K., Pekov I.V., Karpov G.A. and Yapaskurt V.O. (2018b) Hermannjahnite, $CuZn(SO_4)_2$, a new mineral with chalcocyanite derivative structure from the Naboko scoria cone of the 2012–2013 fissure eruption at Tolbachik volcano, Kamchatka, Russia. *Mineralogy and Petrology*, **112**, 123–134.

Siidra O.I., Nazarchuk E.V., Lukina E.A., Zaitsev A.N., Shilovskikh V.V. (2018c) Belousovite, $KZn(SO_4)Cl$, a new sulfate mineral from the Tolbachik volcano with apophyllite sheet-topology. *Mineralogical Magazine*, **82**, 1079–1088.

Siidra, O.I., Nazarchuk, E.V., Zaitsev, A.N. and Shilovskikh, V.V. (2018d) Majzlanite, IMA 2018-016. CNMNC Newsletter No 43, June 2018, page 784; *Mineralogical Magazine*, **82**, 779–785.

Siidra O.I., Borisov A.S., Lukina E.A., Depmeier W., Platonova N.V., Colmont M. and Nekrasova D.O. (2019a) Reversible hydration/dehydration and thermal expansion of euchlorine, ideally $KNaCu_3O(SO_4)_3$. *Physics and Chemistry of Minerals*, **4**, 403–416.

Siidra O.I., Nazarchuk E.V., Zaitsev A.N., Vlasenko N.S. (2019b) Koryakite, $NaKMg_2Al_2(SO_4)_6$, a new anhydrous sulfate mineral from Tolbachik volcano. *Mineralogical Magazine*, DOI: https://doi.org/10.1180/mgm.2019.69

Vergasova L.P. and Filatov S.K. (2012) New mineral species in products of fumarole activity of the Great Tolbachik Fissure Eruption. *Journa of Volcanology and Seismology*, **6**, 281–289.

Wildner M. and Giester G. (1988) Crystal structure refinements of synthetic chalcocyanite ($CuSO_4$) and zincosite ($ZnSO_4$). *Mineralogy and Petrology*, **39**, 201–209.

Zittlau A.H., Shi Q., Boerio-Goates J., Woodfield B.F. and Majzlan J. (2013) Thermodynamics of the basic copper sulfates antlerite, posnjakite, and brochantite. *Geochemistry*, **73**, 39–50.

https://doi.org/10.1180/mgm.2019.68 Published online by Cambridge University Press